ORBIT PROPERTIES OF NON-SCALING FFAG ACCELERATORS USING CONSTANT-GRADIENT MAGNETS

M.K. Craddock (UBC & TRIUMF*) and S.R. Koscielniak (TRIUMF*, Vancouver, B.C., Canada)

Abstract

Very high momentum compaction can be obtained in non-scaling FFAG accelerators using constant-gradient magnets with their field strengths decreasing outwards - sufficiently high that the magnet apertures (and vacuum chamber) need be little wider than in a strong-focusing synchrotron. Such machines are of great potential interest for applications in the 0.1 - 50 GeV energy range requiring higher pulse repetition rates or intensities than synchrotrons can provide. Explicit formulae have been developed for the equilibrium orbit properties, particularly their momentum dependence, in various lattices, and give accurate enough results to provide a useful tool for choosing the magnet parameters. In this paper the dependences of orbit offset and circumference on momentum are explored for doublet lattices, and numerical results from the formulae are compared with those from lattice codes.

INTRODUCTION

For moderate energies Fixed-Field Alternating-Gradient (FFAG) accelerators offer higher repetition rates, acceptance and beam intensity than synchrotrons. Traditional "scaling" FFAGs require the orbit shape, optics and betatron tunes to be kept the same at all energies, to avoid crossing betatron resonances. This places stringent (and non-linear) requirements on the spatial variation of the magnetic field, leading to some engineering challenges.

In recent years, the possibility of dropping the scaling requirement has been explored – in particular for muons, which must be accelerated (and pass through resonances) very quickly. Moreover, using constant-gradient *"linear"* magnets greatly increases dynamic aperture and simplifies construction, while employing the strongest possible gradients minimizes the real aperture. Johnstone *et al.*[1] introduced this *linear non-scaling* approach, showing that it would be very advantageous to use superconducting magnets with positively bending Ds stronger and longer than the Fs (*i.e.* both B_d and $|B_f|$ decrease outwards). The radial orbit spread could be reduced (allowing the use of smaller vacuum chambers and magnets), and the orbit length $C(p)$ shortened and made to pass through a minimum instead of rising monotonically. The variation in orbit period is thereby reduced, allowing the use of high-Q fixed-frequency rf. The minimum in $C(p)$ is obtained by striking a balance between two effects which tend to increase it - larger radii of curvature at high p, and greater orbit scalloping at low p.

Previous work by the authors[2,3] has shown that a simple model, treating the magnets as thin lenses, suffices to derive expressions for the basic orbit shape and its dependence on momentum and other parameters, revealing the parabolic variation of $C(p)$ and the potentiality for very high momentum compaction. For symmetric F0D0 or triplet cells:

$$C(p) = C(p_m) + (12\pi^2/q^2\mu^2N\,\ell)\,(p - p_m)^2$$

where N is the number of cells, q is the charge, μ is the magnet strength (gradient × length - assumed equal for F and D), and ℓ is the (shorter) FD spacing. The orbit radii r show a similar p dependence, though with distinct p_m.

As might be expected from the simplicity of the model, its quantitative predictions do not agree exactly with those obtained using lattice codes such as `MAD`, `COSY`, or `PTC`. For a representative selection of lattices, the agreement as to circumference was found to vary between 1% and 6% for F0D0, but only between 36% and 67% for triplets.

SECTOR-MAGNET MODEL

As it seemed of interest to pursue the analytic approach with something more realistic, but still tractable, we next developed a model assuming constant-gradient sector-magnets set with neighbouring edges parallel. The initial work[4,5], for triplet and F0D0 lattices, gave formulae for orbit radii and circumference yielding values in fair agreement with those produced by the lattice codes (assuming hard-edge magnets). A later paper [6] amplified this work, extending it to sector doublets, and also deriving the explicit momentum dependence of $r(p)$ and $C(p)$.

Here we consider, as well as sector magnets, the use of parallel-ended F and D quadrupoles (as proposed for the NS-FFAG prototype, EMMA [7]), and also report some numerical results for both types of doublet. First, though, we review the sector doublet case. The sector magnets are assumed set with their edges parallel, separated by drifts of length ℓ and L (see Fig. 1), with their opening angles denoted by D and F where $D - F = 2\pi/N$. Note that doublet cells lack the reflection symmetry of triplet or F0D0 cells. The magnet field strengths $B_i = B_{i0} + B_i'x$ (where i stands for f or d) are arranged so that for some reference momentum $p_0 = qB_{d0}\,d = qB_{f0}\,f$ the closed equilibrium orbit (CEO)

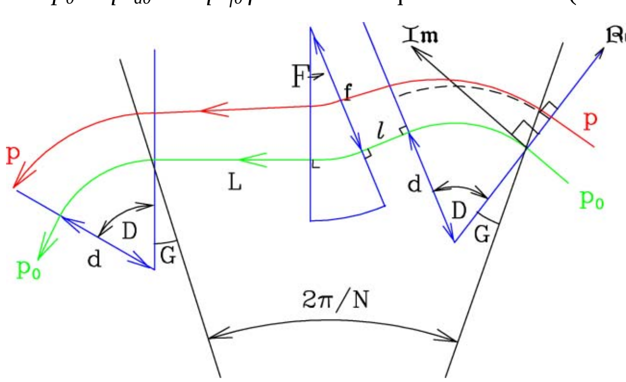

Figure 1: Orbits in a sector doublet cell.

*TRIUMF receives federal funding under a contribution agreement through the National Research Council of Canada.

1-4244-0917-9/07/$25.00 ©2007 IEEE

follows a centred circular arc of radius $\rho_{i0} = d$ or f within each magnet, entering and leaving each edge perpendicularly. Radial displacements x are measured relative to this "reference orbit".

The geometric parameters of the reference orbit may be conveniently described in a complex plane centred at its entry point into the D magnet, with the real axis outwards along the sector edge, at an angle G with respect to the radius vector (length R) from the machine centre. Following the orbit the length of the cell, it may be seen that:

$$Re^{-iG}(e^{2\pi i/N} - 1) = -d + (d + f + i\ell)e^{iD} - (f - iL)e^{2\pi i/N},$$

providing two real equations which may be solved for the angle G, and one of D, d, or f, given the other two and N, R, ℓ and L.

For other momenta $p = p_0 + \Delta p$ there are also local EOs within each magnet - circular arcs displaced from the reference orbit $x = 0$ by $X_f(p)$ and $X_d(p)$ where

$$X_i(p) = \frac{\rho_{i0}}{2n_{i0}}\left\{-|1-n_{i0}| + \sqrt{(1-n_{i0})^2 - 4n_{i0}(\Delta p/p_0)}\right\}$$

Here the field indices $n_{d0} \equiv -B_d'd/B_{d0}$ and $n_{f0} \equiv +B_f'f/B_{f0}$. Within each magnet the CEO follows a betatron oscillation (sinusoidal in F, hyperbolic in D) of amplitude A_f or A_d about the local EO for that momentum.

If the phase advances at the ends of the long straight are denoted ψ_L and ϕ_L, the betatron displacements and divergences at the magnet edges are:

$$x_{fL} - X_f = A_f \cos\phi_L, \qquad x_{dL} - X_d = A_d \cosh\psi_L,$$
$$\tan\chi_{fL} = A_f\lambda_f \sin\phi_L, \qquad \tan\chi_{dL} = A_d\lambda_d \sinh\psi_L.$$

$$x_f - X_f = A_f \cos(\phi+\phi_L), \quad x_d - X_d = A_d \cosh(\psi+\psi_L),$$
$$\tan\chi_f = A_f\lambda_f \sin(\phi+\phi_L), \quad \tan\chi_d = A_d\lambda_d \sinh(\psi+\psi_L),$$

where the phase advances and divergence

$$\phi \equiv \sqrt{1-n_f}\,F, \quad \psi \equiv \sqrt{n_d - 1}\,D, \quad \tan\chi = \frac{1}{\rho}\frac{d\rho}{d\theta},$$

and $\lambda_f \equiv \sqrt{(1 - n_f)}/f$, $\lambda_d \equiv \sqrt{(n_d - 1)}/d$, and n_f, n_d are evaluated at X_f, X_d.

Writing $C_d \equiv A_d \cosh\psi_L$, $S_d \equiv A_d \sinh\psi_L$,

$C_f \equiv A_f \cos\phi_L$, $S_f \equiv A_f \sin\phi_L$,

$\Delta X \equiv X_f - X_d$,

and matching the divergences and displacements over the two drifts, so that:

$\chi_f = \chi_d \equiv \chi_{fd}$, $\quad x_f - x_d = \ell \tan\chi_{fd}$,

$\chi_{fL} = \chi_{dL} \equiv \chi_{fdL}$ $\quad x_{fL} - x_{dL} = \ell \tan\chi_{fdL}$,

yields four linear equations in C_d, S_d, C_f, S_f:

$$\lambda_f S_f = \lambda_d S_d = -(C_f - C_d + \Delta X)/L$$

$$\lambda_f(S_f\cos\phi + C_f\sin\phi) = \lambda_d(S_d\cosh\psi + C_d\sinh\psi)$$

$$= (\Delta X + C_f\cos\phi - S_f\sin\phi - C_d\cosh\psi - S_d\sinh\psi)/\ell.$$

The solutions are:

$$C_d = (\Delta X/M)\{(1-\cos\phi)(1+\cosh\psi) + \lambda_f(L+\ell\cosh\psi)\sin\phi + (\lambda_f/\lambda_d)\sin\phi\sinh\psi\}$$

$$C_f = (\Delta X/M)\{(1+\cos\phi)(\cosh\psi-1) + \lambda_d(L+\ell\cos\phi)\sinh\psi + (\lambda_d/\lambda_f)\sin\phi\sinh\psi\}$$

$$S_d = (\Delta X/M)\{(\cos\phi-1)\sinh\psi - \lambda_f\,\ell\sin\phi\sinh\psi + (\lambda_f/\lambda_d)(1-\cosh\psi)\sin\phi$$

$$S_f = (\Delta X/M)\{(1-\cosh\psi)\sin\phi - \lambda_d\,\ell\sin\phi\sinh\psi - (\lambda_d/\lambda_f)(1-\ell\cos\phi\sinh\psi)$$

$$M = 2(1-\cos\phi\cosh\psi) + (\ell+L)(\lambda_f\cosh\psi\sin\phi - \lambda_d\cos\phi\sinh\psi) + \lambda_d\lambda_f\,\ell L\sin\phi\sinh\psi + [(\lambda_f/\lambda_d)-(\lambda_d/\lambda_f)]\sin\phi\sinh\psi.$$

These can be used to obtain explicit formulae for A_d, ψ_L, A_f, and ϕ_L, and to compute the offsets $x(p,\theta)$ for any azimuthal angle θ. We can also integrate along the various orbit segments (F, ℓ, D, L) to find the deviations in path length between momenta p and p_0 (ignoring negligible higher-order terms in A_f/f and A_d/d):

$$\Delta s_f \cong -(X_f + C_f)F + \frac{A_f}{\sqrt{1-n_f}}[\phi - \sin(\phi+\phi_L) + \sin\phi_L]$$
$$+\frac{1}{8}\lambda_f A_f^2[2\phi - \sin 2(\phi+\phi_L) + \sin 2\phi_L]$$
$$\Delta s_d \cong (X_d + C_d)D + \frac{A_d}{\sqrt{n_d - 1}}[\sinh(\psi+\psi_L) - \sinh\psi_L - \psi]$$
$$+\frac{1}{8}\lambda_d A_d^2[\sinh 2(\psi+\psi_L) - \sinh 2\psi_L - 2\psi]$$
$$\Delta s_\ell = \ell(\sec\chi_{fd} - 1), \qquad \Delta s_L = L(\sec\chi_{fdL} - 1).$$

Table 1 compares values of x_{fL}, x_{dL} and $\Delta C = N\,\Sigma\Delta s_i$ computed for sector doublet lattices designed by Berg[8] and Koscielniak and Johnstone [9] with those obtained by tracking. While the agreement is good for the offsets (<5% discrepancy), it is less so for ΔC, particularly for p_{min}. ΔC seems especially sensitive to small errors in the amplitudes A_d and A_f; if these are adjusted to give exact agreement with the tracked offsets (tabulated as ΔC^*), the discrepancies drop to 5-10%. The basic source of error is probably the use of n_i values computed at the local EO, which differ significantly from those on the orbit segment.

Table 1: Formulae (yellow) & tracking (blue) compared.

	Sectors[8]		**Sectors[9]**		**Quadrupoles**	
C (m)	436.5		15.54		16.57	
N	101		42		42	
E (MeV)	10,000	20,000	10	20	10	20
x $_{dL}$ (mm)	3.2	39.2	-1.3	5.5	-0.6	7.3
Tracked	5.3	39.7	-3.3	6.6	0.1	7.5
x $_{fL}$ (mm)	-26.8	68.6	-8.4	9.4	-8.3	11.9
Tracked	-27.6	73.5	-8.8	9.0	-6.3	12.3
ΔC (mm)	166	237	20	41	30	45
ΔC* (mm)	195	206				
Tracked	211	217	34	34	37	37

QUADRUPOLE DOUBLET

An alternative to sectors is to use parallel-ended constant-gradient F and D magnets (lengths L_f, L_d) - i.e. quadrupoles where the trajectories all lie to one side of their axes (not necessarily coincident), so that they provide both focusing and bending. We follow the arrangement proposed for EMMA [7] where the F and D axes are set parallel. No reference orbit or momentum is defined by the orbit geometry; instead an N-sided reference polygon is defined close to the mid-momentum CEO, with the F and D axes for each cell set parallel to one of the sides, offset by X_F and X_D respectively (Fig. 2). Displacements $x(p,z)$ are measured relative to the reference polygon. The figure clearly illustrates how the greater wiggle in the low-energy orbits enables their circumference to match that of the high-energy ones at larger radius.

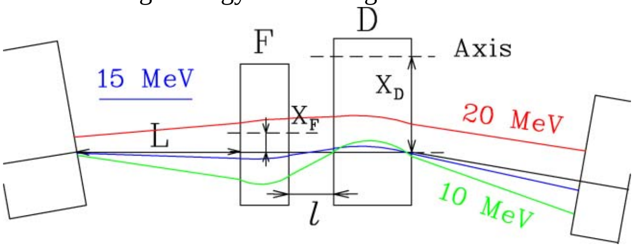

Figure 2: Orbits in a quadrupole doublet cell.

As before, the CEO for each momentum is made up of sinusoidal, hyperbolic and straight segments. Writing $k_f \equiv \sqrt{(q|B_f'|/p)}$, $k_d \equiv \sqrt{(q|B_d'|/p)}$, and $\phi \equiv k_f L_f$, $\psi \equiv k_d L_d$, then the displacements and divergences at the magnet edges are given by:

$$X_F - x_{fL} = A_f \cos\phi_L, \qquad X_D - x_{dL} = A_d \cosh\psi_L,$$
$$\tan\chi_{fL} = k_f A_f \sin\phi_L, \qquad \tan\chi_{dL} = k_d A_d \sinh\psi_L.$$

$$X_F - x_f = A_f \cos(\phi+\phi_L), \quad X_D - x_d = A_d \cosh(\psi+\psi_L),$$
$$\tan\chi_f = k_f A_f \sin(\phi+\phi_L), \quad \tan\chi_d = k_d A_d \sinh(\psi+\psi_L),$$

Matching displacements and divergences, we find four equations for $C_f \equiv A_f \cos\phi$, etc., very similar to those above, but in two cases now non-linear:

$$\arctan(k_f S_f) = \arctan(k_d S_d) - 2\pi/N;$$
$$k_f S_f\,[L + (X_D - C_d)\sin(2\pi/N)] = X_F - C_f - (X_D - C_d)\cos(2\pi/N);$$
$$k_f(S_f \cos\phi + C_f \sin\phi) = k_d(S_d \cosh\psi + C_d \sinh\psi)$$
$$= (X_F - X_D + C_f \cos\phi - S_f \sin\phi - C_d \cosh\psi - S_d \sinh\psi)/\ell.$$

Explicit solutions to these equations have not been found for the general case, although S_d, C_d and C_f can be expressed fairly simply in terms of S_f. Numerical solutions can be found, however, allowing A_d, ψ_L, A_f, ϕ_L, and the offsets $x(p,z)$ to be calculated, and are discussed below.

Integrating along the various orbit segments (L_D, ℓ, L_F, L) to find the deviations in path length between momenta, we find:

$$\Delta s_f \cong +\frac{1}{8} k_f A_f^2 \left[2\phi - \sin 2(\phi+\phi_L) + \sin 2\phi_L\right]$$
$$\Delta s_d \cong +\frac{1}{8} k_d A_d^2 \left[\sinh 2(\psi+\psi_L) - \sinh 2\psi_L - 2\psi\right]$$
$$\Delta s_\ell = \ell(\sec\chi_{fd} - 1), \qquad \Delta s_L = [L + (X_d - C_d)\sin(2\pi/N)]\sec\chi_{fL} - L.$$

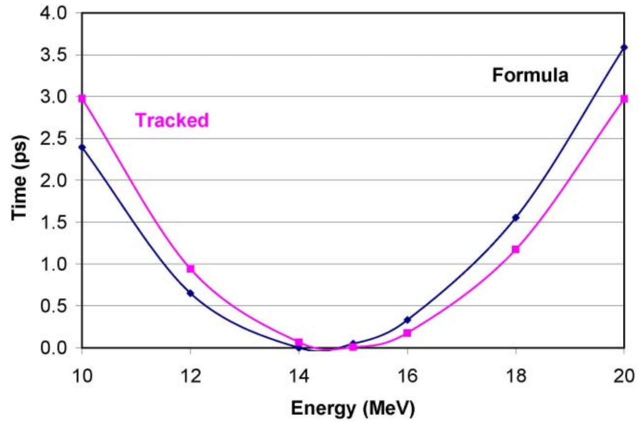

Figure 3: Energy variation of time of flight in one cell.

The formulae for x_{fL}, x_{dL} and $\Delta C = N\,\Sigma\Delta s_i$ have been evaluated for the current EMMA baseline lattice[10], and the results are shown in Table 1, along with those obtained by tracking. Considering that the latter included fringing field effects, while our model assumes hard-edge magnets, the agreement is remarkably close. Fig. 3 shows the energy variation of time of flight $\Delta s/\beta c$ through one cell. Just as for the sector magnets, there is a tendency for the model to underestimate the path and time differences at low energy, and overestimate them at high energy.

CONCLUSIONS

The hard-edge magnet model presented here for linear non-scaling FFAGs with doublet lattices cannot supplant orbit tracking codes for accurate determination of the orbit properties. It does, however, provide a simple tool to assist in the choice of magnet parameters in the early stages of machine design.

REFERENCES

[1] C. Johnstone, W. Wan, A. Garren, PAC'99, 3068.
[2] M.K. Craddock, FFAG 2003 Workshop, BNL; http://www.cap.bnl.gov/mumu/conf/ffag-031013/Craddock.pdf.
[3] S. Koscielniak, M. Craddock, EPAC'04, 1138 (2004).
[4] M.K. Craddock, FFAG 2004 Workshop, TRIUMF, http://www.triumf.ca/ffag2004/programme.html; S. Koscielniak, *ibid.*
[5] S. Koscielniak, EPAC'04, 1138 (2004).
[6] M. Craddock, S. Koscielniak, EPAC'06, 1666 (2006).
[7] T.R. Edgecock, PAC'07, THOBAB01.
[8] J.S. Berg, FFAG 2003, Brookhaven, http://www.cap.bnl.gov/mumu/conf/ffag-031013/Berg2.pdf
[9] S.R. Koscielniak, C. Johnstone, PAC'05, 3173 (2005).
[10] J.S. Berg *et al.*, PAC'07, THPMS083.